Numerical simulations of cone penetration response via accounting for state-dependence and full-strain-range non-linearity of sand

Senjie Tong[1,2], *Maosong* Huang[1], *Zhenhao* Shi[1#], *Jian* Yu[1], *Bin* Wang[2], *Changjiang* Sun[2]

[1]*Department of Geotechnical Engineering, Tongji University, 1239 Siping Road, Shanghai, China*
[2] *POWERCHINA Huadong Engineering Corporation, 201 Gaojiao Road, Hangzhou, China*
[#]*1018tjzhenhao@tongji.edu.cn*

ABSTRACT

The penetration response of CPT is not only related to the stress and density states of sand but also influenced by the non-linear stress-strain relations of soils from very small (10^{-5}) to relatively large (10^{-1}) strain levels. Appropriate considerations of the above key soil behaviours can be crucial for accurate numerical simulations of CPT response. For this purpose, an intergranular strain (IGS)-based elastic model is introduced into a critical-state-based, state-dependent plasticity model to capture the state-dependence and full-strain-range non-linearity behaviour of sand. A numerical model of the CPT penetration process is then established by combining the aforementioned constitutive model and the arbitrary Lagrangian-Eulerian (ALE) large deformation finite element technique. The latter is adopted to handle the problems of large deformations of soil and mesh distortion. Then the computed response of CPT is compared against centrifuge test observations, and the numerical model is utilized to analyse the influences of the full-strain-range non-linearity behaviour of sand on the penetration response of CPT. The results indicate that the non-linear stress-strain relations at small strains can have noticeable impacts on the tip resistance of CPT, in particular for loose sand, while having a relatively small influence on the penetration depth required to reach a steady-state penetration resistance. The above influences might be attributed to a rapid decay of soil strains with the distance from the cone tip, and consequently high stiffness and strong constraints effects of far-field soils on core soils adjacent to the cone tip.

Keywords: CPT; numerical simulations; state-dependent model; small strain stiffness; sand.

1. Introductions

The cone penetration test (CPT) is an important in-situ test for evaluating the site-specific mechanical parameters of sand, like density, stiffness, and strength (Jamiolkowski et al. 2003; Lee et al. 2010). Abilities to realistically simulate CPT penetration response can be useful for interpreting in-situ CPT data and consequent site characterization. The penetration response of CPT is not only related to the stress and density states of sand but also influenced by the non-linear stress-strain relations of soils from very small (10^{-5}) to relatively large (10^{-1}) strain levels (Lee et al. 2009; Lee et al. 2011; Ahmed 2017). Appropriate considerations of the above key soil behaviours can be crucial for accurate numerical simulations of CPT response.

The goal of this work is to analyse the impacts of the non-linear stress-strain relations of soils from very small (10^{-5}) to relatively large (10^{-1}) strain levels on the CPT response. For this purpose, an intergranular strain (IGS)-based elastic model is introduced into a critical-state-based, state-dependent plasticity model to capture the state-dependence and full-strain-range non-linearity behaviour of sand. The calibrations of adopted model parameters as well as the model performance are presented. A numerical model for the CPT penetration is then established by combining the aforementioned constitutive model and the arbitrary Lagrangian-Eulerian (ALE) large deformation finite element technique. Finally, the numerical model is utilized to analyse the influences of the full-strain-range non-linearity behaviour of sand on the cone penetration response.

2. Constitutive model formulation

In this section, the framework of the critical-state-based, state-dependent plastic model and intergranular strain (IGS)-based elastic model will be described. The former controls the stress-strain behaviour of sand under a relatively large strain (10^{-3}~ 10^{-1}) level, while the latter is introduced to simulate the elastic response under a very small strain ($<10^{-3}$) level. Then, the calibrations of model parameters and the verification of the model will be discussed.

2.1. State-dependent baseline model for sand

The critical-state-based, state-dependent plastic model used in this study is a modified Li and Dafalias (2000) model for sand. This model takes into account the state parameter proposed by Been and Jefferies (1985), allowing it to accurately represent the behaviour of sand that is either looser or denser than the critical state. The state parameter is defined as:

$$\psi = e - e_c \tag{1}$$

where e is the current void ratio and e_c is the void ratio on the critical state line that corresponds to the current effective mean normal stress:

$$e_c = e_\Gamma - \lambda_c \left(\frac{p}{p_a} \right)^{\xi_c} \tag{2}$$

where $p = \sigma_{ii}/3$ is the effective mean stress, while e_Γ, λ_c, and ξ_c are model parameters that control the shape and location of the critical state line. It is seen that the loose and dense states relative to the critical state indicate the $\psi > 0$ and $\psi < 0$, respectively.

The soil model includes a general cone-shaped yield surface with a deviatoric hardening mechanism. Both plastic dilatancy and strain hardening are explicit functions of the aforementioned state parameter, thus accounting for barotropic and torsional effects in granular soils. For a more comprehensive discussion of the model formulation and verification, please refer to the work by Huang et al. (2021).

2.2. Intergranular strain elastic model

The aforementioned fundamental state-dependent constitutive model governs the plastic behavior of the granular soil, while the corresponding elastic response is controlled by the intergranular strain (IGS) elastic model developed by Shi and Huang (2020). The intergranular strain elastic model considers the amplification of soil stiffness during the small-strain phase through the interpolation function m_s. It further diminishes the stiffness by taking into account the cumulative intergranular strain, enabling the decay of soil stiffness with increasing strain accumulation. Consequently, the elastic shear modulus G is defined as:

$$G = m_s G_l \tag{3}$$

where G_l is the elastic shear modulus at the large-strain phase, which is defined according to Richart et al (1970) as follows:

$$G_l = G_l^{ref} \frac{(2.97 - e)^2}{1 + e} \sqrt{\frac{p}{p_a}} \tag{4}$$

where G_l^{ref} represents the reference value for G_l, and p_a is the atmospheric pressure. After determining G, the bulk modulus K can be calculated using Poisson ratio ν based on isotropic linear elasticity theory:

$$K = G \frac{2(1+\nu)}{3(1-2\nu)} \tag{5}$$

The interpolation function m_s is used to calculate the elastic modulus based on the rotation of the strain path θ_r (which represents the angle between the direction of strain rate and intergranular strain) and the normalized intergranular strain amplitude ρ. The $\rho = \|\zeta_{ij}\| / R_{\max}$ is obtained by dividing the intergranular strain ζ_{ij} by the maximum intergranular strain value $R_{\max}$. The definition of the interpolation function m_s is based on the work of Shi and Huang (2020):

$$m_s = \rho^\chi m_T + \left(1 - \rho^\chi\right) m_R + \begin{cases} \rho^\chi (1 - m_T) |l|^{n_s} & (l > 0) \\ \rho^\chi (m_R - m_T) |l|^{n_s} & (l \le 0) \end{cases} \tag{6}$$

where χ, m_R, m_T, and n_s are model parameters, where $m_R = G_0 / G_l$ defines the ratio of the elastic shear modulus at very small strain level to the elastic shear modulus in the large strain stage, and m_T is the shear modulus amplification when θ_r is 90°. The $l = \hat{\zeta}_{ij} \hat{\dot{\varepsilon}}_{ij}$ denotes the projection of the unit strain increment along the direction of intergranular strain, where $\hat{\zeta}_{ij} = \zeta_{ij} / \|\zeta_{ij}\|$ and $\hat{\dot{\varepsilon}}_{ij} = \dot{\varepsilon}_{ij} / \|\dot{\varepsilon}_{ij}\|$. The $\dot{\varepsilon}_{ij}$ represents the tensor of strain rate. The parameters n_s controls the variation m_s with θ_r, as shown in Fig. 1. The G_0 is the elastic shear modulus at a very small strain which the definition is the same as Equation (4):

$$G_0 = G_0^{ref} \frac{(2.97 - e)^2}{1 + e} \sqrt{\frac{p}{p_a}} \tag{7}$$

where G_0^{ref} represents the reference value of G_0.

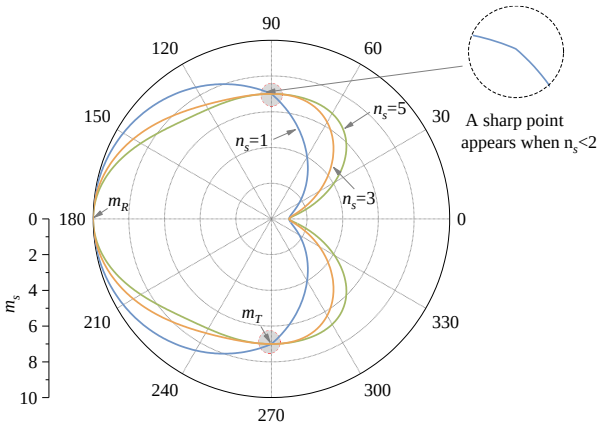

Figure 1 The relationship between the interpolation function m_s and the rotation of the strain path θ_r, where $m_R = 10$ and $m_T = 7$.

The evolution of intergranular strain is dependent on the direction between strain rate and intergranular strain. According to Niemunis and Herle (1997), the definition of increment intergranular strain is:

$$\dot{\zeta}_{ij} = \begin{cases} \dot{\varepsilon}_{ij} - \rho^{\beta_r} l \|\dot{\varepsilon}_{mn}\| \hat{\zeta}_{ij} & (l > 0) \\ \dot{\varepsilon}_{ij} & (l \le 0) \end{cases} \tag{8}$$

where β_r is a model parameter.

2.3. Model calibration

The state-dependent plastic constitutive model has 12 parameters which the comprehensive calibration process can be found in Li and Dafalias (2000).

As the calibration of IGS model parameters, the main objective is to determine G_0^{ref}, m_R, and m_T. The G_0^{ref} represents the initial value of the small-strain elastic shear modulus. According to the definition of m_R, m_R can be determined by the ratio of G_0^{ref} to G_l^{ref}. The m_T is calculated by $m_{mat} = m_T / m_R$.

Regarding the calibration of parameters R_{max}, χ, and β_r, this paper utilized the modified Hardin-Drnevich hyperbolic modulus degradation curve (Dos Santos and Correia, 2001) as a baseline, which describes the variation of shear modulus with strain through the utilization of the parameter $\gamma_{0.7}$ (i.e., the shear strain at which the shear modulus diminishes to 0.7 times the initial shear modulus). By searching the optimized relationship between variables R_{max}, χ, β_r, and $\gamma_{0.7}$, the above-mentioned parameters can be determined once the parameter $\gamma_{0.7}$ is obtained from experimental tests.

The calibrated parameters for Toyoura sand of the IGS-based state-dependent constitutive model can be found in Table 1 and the corresponding model performance is shown in Figure 2. It can be seen that the model can reasonably represent the variation of shear stiffness at small strains.

Table 1 Model parameters for Toyoura sand

Elastic parameters	IGS parameters	Critical state parameters	Dilatancy parameters	Hardening parameters
$G_l^{ref}=17.2$Mpa	$G_0^{ref}=39$MPa	$M_c=1.25$	$d_0=0.88$	$h_1=2.89$
$v=0.05$	$\gamma_{0.7}=3.75$E-5	$e_\Gamma=0.934$	$m=2.5$	$h_2=2.80$
	$n_s=3.0$	$\lambda_c=0.019$		$n=1.1$
	$m_{mat}=0.6$	$\xi_c=0.7$		
		$c=0.75$		

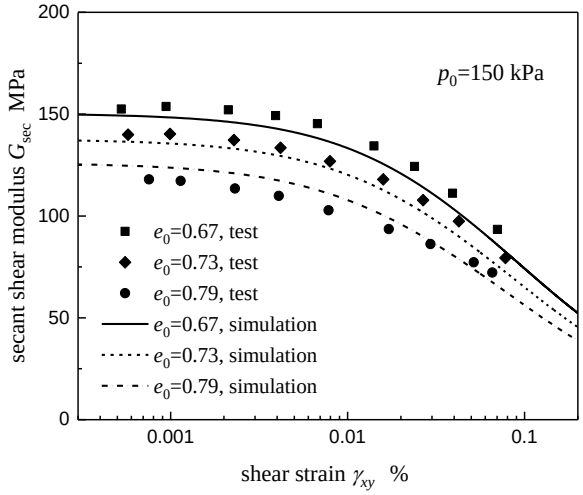

Figure 2 Comparisons of normalized shear modulus degradation relations between tested and simulated results.

3. Analysis of full-strain-range behavior of sand on CPT response

3.1. CPT model

Figure 3 depicts the geometry and mesh of the CPT model used in the simulations. The axisymmetry of the problem is exploited (i.e., only a slice of the soil mass is modeled and the left boundary of the model represents the axis of symmetry). The cone with an angle of 60° and the probe with a diameter of 3.57cm is simulated by using a rigid body. According to the experimental findings by Uesugi and Kishida (1986), the friction between Toyoura sand and relatively smooth steel is approximately 0.4. Thus, the friction coefficients between the interface of the cone and the soil, as well as between the probe and the soil, are both set to 0.4. The soil is simulated by the IGS-based state-dependent model. The simulated soil range has a width of 0.9 meters, which is 50 times the cone radius. Been et al. (1986) has concluded from extensive experiments that the model width for loose sand samples should be greater than 20 times the cone diameter, while for dense sand, it should be larger than 50 times the cone diameter to eliminate boundary effects significantly. The model height is 1.5m, and the penetration depth is 1.08m, approximately 30 times the cone diameter. The penetration velocity is set at 2cm/s. To prevent soil elements on the symmetry axis from intruding to the left side and allow smooth movement onto the cone surface, a smooth rigid plate (Figure 3b) is placed at the lower end of the cone during the penetration simulation. This rigid plate does not affect the surrounding soil during the penetration process due to its smooth properties.

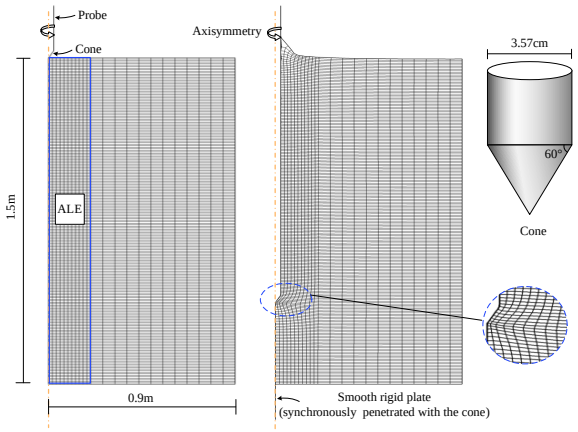

(a) before penetration (b) after penetration

Figure 3 Geometry and mesh of numerical CPT model.

As shown in Figure 3a, a mesh consisting of 7456 four-node reduced-integration elements (CAX4R) is employed in Abaqus/ Explicit. The blue dashed box in Figure 3 represents the region where the Arbitrary Lagrangian Eulerian adaptive meshing (ALE) is applied to improve the distortion of Lagrangian grids during penetration. The deformed mesh is shown in Figure 3(b), indicating the effectiveness of the ALE in solving mesh distortion issues.

3.2. Verification of model performance

The CPT tests conducted by Fioravante et al. (1991) are employed to validate the accuracy of the numerical CPT model. These tests are carried out under 1g condition and Toyoura sand was used as the experimental material. The adopted model parameters for Tyoura sand are summarized in Table 1. Two sets of test samples with initial relative densities of 57% and 86% are used, along with initial stresses of $\sigma_v=111$kPa, $\sigma_h=61$kPa and $\sigma_v=61$kPa, $\sigma_h=30$kPa. The initial relative density and stress conditions in the simulations are the same as those in the actual tests.

Table 2 summarises comparisons between the measured results and the predicted results. The fact that the predicted tip resistances closely match the measured

results suggests that the proposed CPT model exhibits a high level of reliability.

Table 2 Comparison between the measured and computed response of Toyoura sand from CPT tests (Test data after Fioravante (1991))

Sand	σ_v kPa	σ_h kPa	D_r %	Measured q_c MPa	Predicted q_c MPa
Toyoura	111	60	86	23.6	23.9
Toyoura	61	30	57	8.2	8.9

3.3. Influence of small-strain behaviour of sand

In this section, the influence of the small-strain behaviour of sand on the CPT response is analyzed and the model parameters for Toyoura sand are used. Due to space limitation, only tip resistance is analyzed while a comprehensive interpretation of the CPT results including sleeve friction will be presented in detail in the forthcoming research.

Figure 4 shows the relationship between the tip resistance and the penetration depth of CPT, where the initial relative density of the soil is 30% and 70%, and the initial effective mean stress is 100kPa and 300kPa. It indicates that the normalized penetration depth required for the tip resistance to reach a stable state is related to the initial state of the soil, which decreases with the increase of the initial relative density but decreases with decrease of initial effective mean stress.

Figure 4 further illustrates how the small-strain behaviour of sand affects the response of cone penetration tests (CPT). The findings indicate that despite cone penetration being associated with large deformation issues, considering the small strain properties of sand can noticeably enhance the tip resistance. The above influences might be attributed to a rapid decay of soil strains with the distance from the cone tip, and consequently high stiffness and strong constraints effects of far-field soils on core soils adjacent to the cone tip. Moreover, Fig. 4 suggests that the influences of small-strain stiffness on penetration resistance are more sensitive to the density of sand than confining stresses. Specifically, as the initial relative density of sand decreases, the influence of small-strain behaviour becomes more notable. This is evident from the fact that the tip resistance increases by 10.3% and 10.1% for loose sand with initial vertical effective stress (p_0) of 100kPa and 300kPa, respectively. While the tip resistance rises by 7.6% and 7.3% for dense sand with p_0=100kPa and 300kPa, correspondingly.

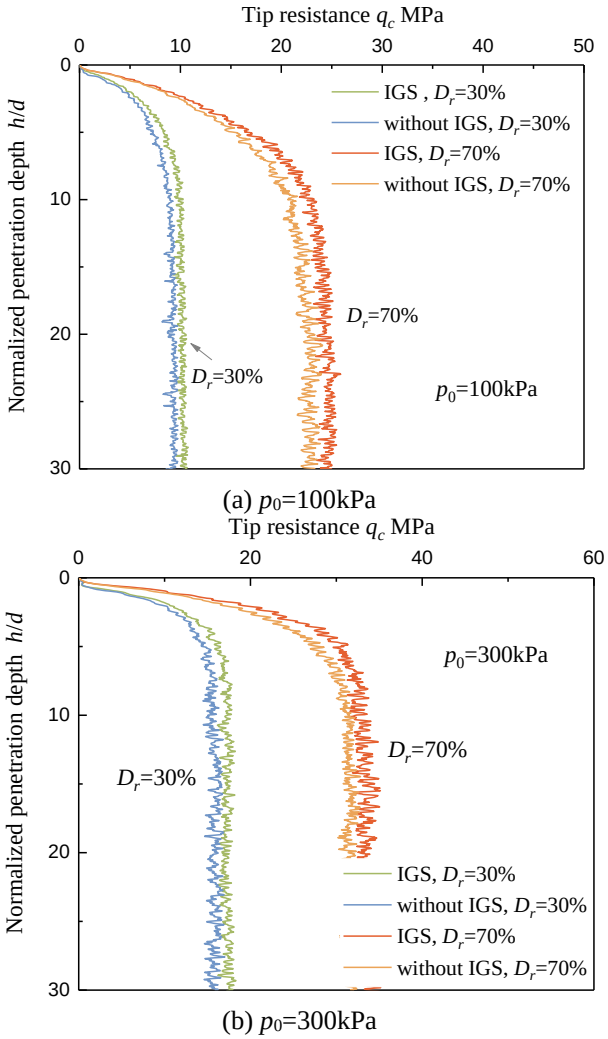

Figure 4 Comparison of tip resistance between the constitutive model with or without considering small strain stiffness.

4. Conclusions

This work aims +to investigate the effects of small-strain stiffness properties on the response of cone penetration tests (CPT) in sand. To achieve this, an intergranular strain (IGS)-based elastic model is introduced into a critical-state-based, state-dependent plasticity model and this model effectively describes the state-dependence and full-strain-range non-linearity behavior of sand. Subsequently, A numerical model of the CPT penetration process is then established by combining the aforementioned constitutive model and the ALE large deformation finite element technique. By comparing the simulations with 1g CPT tests, the reliability of the simulations is confirmed. This study further analyzes the impact of small-strain behavior on penetration response in sand. The following main conclusions can be drawn from this work:

(1) The normalized penetration depth required for the tip resistance to reach a stable state is related to the initial state of the soil, which decreases with the increase of the initial relative density but decreases with decrease of initial effective mean stress.

(2) The small strain properties of sand can noticeably enhance the tip resistance. Moreover,

the tip resistance rises about 10.3% and 7.6% for loose and dense sand correspondingly, indicating a more notable influence of small-strain behaviour of sand as the initial relative density decreases.

(3) The influences of the small strain properties of sand on tip resistance might be attributed to a rapid decay of soil strains with the distance from the cone tip, and consequently high stiffness and strong constraints effects of far-field soils on core soils adjacent to the cone tip.

Acknowledgments

The authors are grateful for the financial support provided by the National Natural Science Foundation of China (No. 11972260).

References

Ahmed, S. M. 2017. "Enhancing the CPT Correlation With the Small Strain Shear Stiffness of Sands." Ain Shams Engineering Journal, 8(4): 539-548. http://doi.org/10.1016/j.asej.2016.08.010

Been, K., Jefferies, M. G. 1985. "A State Parameter for Sands." Geotechnique, 35(2):99–112. http://doi.org/10.16285/j.rsm.2016.1237

Been, K., Crooks, J. H. A., Becker, D. E., et al. 1986. "The Cone Penetration Test in Sands: Part I, State Parameter Interpretation." Geotechnique, 36(2): 239-249. http://doi.org/10.1680/geot.1986.36.2.239

Dos Santos, J. A., Correia, A. G. 2001. "Reference Threshold Shear Strain of Soil. Its Application to Obtain an Unique Strain-dependent Shear Modulus Curve for Soil." In: Proceedings of the Fifteenth International Conference on Soil Mechanics and Geotechnical Engineering, Istanbul, Turkey, 1-3, 267-270.

Fioravante, V., Jamiolkowski, M., Tanizawa, F., et al. 1991. "Results of CPTs in Toyoura Quartz Sand." In: Proceedings of the 1st International Symposium on Calibration Chamber Testing (ISOCCT-1), Potsdam, New York, 135-146.

Hong, Y., Koo, C. H., Zhou, C., et al. 2017. "Small Strain Path-dependent Stiffness of Toyoura Sand: Laboratory Measurement and Numerical Implementation." International Journal of Geomechanics, 17(1): 04016036. https://doi.org/10.1061/(ASCE)GM.1943-5622.0000664

Huang, M., Tong, S., Shi, Z. 2021. "Solution for Spherical Cavity Expansion in State-dependent Soils." Acta Geotechnica, 16: 1773-1788. https://doi.org/10.1007/s11440-020-01096-3

Jamiolkowski, M., Lo Presti, D. C. F., Manassero, M. 2003. "Evaluation of Relative Density and Shear Strength of Sands from CPT and DMT." Soil Behavior and Soft Ground Construction, 201-238. https://doi.org/10.1061/40659(2003)7

Lee, J., Kyung, D., Kim, B., et al. 2009. "Estimation of the Small-strain Stiffness of Clean and Silty Sands Using Stress-strain Curves and CPT Cone Resistance." Soils and Foundations, 49(4): 545-556. https://doi.org/10.3208/sandf.49.545

Lee, M. J., Hong, S. J., Choi, Y, M., et al. 2010. "Evaluation of Deformation Modulus of Cemented Sand Using CPT and DMT." Engineering Geology, 115(1-2): 28-35. https://doi.org/10.1016/j.enggeo.2010.06.016

Lee, M. J., Choi, S. K., Kim, M. T., et al. 2011. "Effect of Stress History on CPT and DMT Results in Sand." Engineering Geology, 117(3-4): 259-265. https://doi.org/10.1016/j.enggeo.2010.11.005

Li, X. S., Dafalias, Y. F. 2000. "Dilatancy for cohesionless soils." Geotechnique, 50(4):449–460. https://doi.org/10.1680/geot.2000.50.4.449

Niemunis, A., Herle, I. 1997. "Hypoplastic Model for Cohesionless Soils With Elastic Strain Range." Mechanics of Cohesive-frictional Materials: An International Journal on Experiments, Modelling and Computation of Materials and Structures, 2(4): 279-299. https://doi.org/10.1002/(SICI)1099-1484(199710)2:4<279::AID-CFM29>3.0.CO;2-8

Richart, F. E., Hall, J, R., Woods, R, D. 1970. "Vibrations of Soils and Foundations. In: International Series in Theoretical and Applied Mechanics." Prentice-Hall, Englewood Cliffs.

Shi, Z., Huang, M. 2020. "Intergranular-strain Elastic Model for Recent Stress History Effects on Clay." Computers and Geotechnics, 118: 103316. https://doi.org/10.1016/j.compgeo.2019.103316

Uesugi, M., Kishida, H. 1986. "Frictional resistance at yield between dry sand and mild steel." Soils and Foundations, 26(4): 139-149.